Resilient Smart Power Grid Synchronization Estimation Method for System Resilience with Partial Missing Measurements

Yi Wang, *Member*, *IEEE*, Yanxin Liu, Mingdong Wang, *Member*, *IEEE*, Venkata Dinavahi, *Fellow*, *IEEE*, Jun Liang, *Fellow*, *IEEE*, and Yonghui Sun, *Member*, *IEEE*

***Abstract*—With the increasing demand for power system stability and resilience, effective real-time tracking plays a crucial role in smart grid synchronization. However, most studies have focused on measurement noise, while they seldom think about the problem of measurement data loss in smart power grid synchronization. To solve this problem, a resilient fault-tolerant extended Kalman filter (RFTEKF) is proposed to track voltage amplitude, voltage phase angle and frequency dynamically. First, a three-phase unbalanced network's positive sequence fast estimation model is established. Then, the loss phenomenon of measurements occurs randomly, and the randomness of data loss's randomness is defined by discrete interval distribution [0, 1]. Subsequently, a resilient fault-tolerant extended Kalman filter based on the real-time estimation framework is designed using the time-stamp technique to acquire partial data loss information. Finally, extensive simulation results manifest the proposed RFTEKF can synchronize the smart grid more effectively than the traditional extended Kalman filter (EKF).**

***Index Terms*—Dynamic state estimation, Kalman filter, partial missing measurements, power systems, smart grid, synchronized measurements.**

I. Introduction

In recent years, significant changes have occurred in the-power grid [1], [2]. On the one hand, there has been an increase in the integration rate into renewable energy generation. on the other hand, intelligent load control, energy storage and new energy vehicles are also widely deployed [3]. This evolution will provide stochastic operating behavior and enhance the power grid's dynamic properties. At the same time, so issues like the rising demand for electricity and the greenhouse effect can be adequately addressed, public policy goals have been developed by various governments. For instance, in developing new energy installed capacity, by 2030, China's total installed power capacity will increase to 3.8 billion kilowatts, and the proportion of clean energy installed capacity will reach 68%. It is not hard to predict that the deployment of distributed generation systems (DPGS) will increase at a high rate of speed due to the need to produce more clean energy [4]. As a key factor in accurately controlling grid-connected converters and DPGS, grid synchronization with high accuracy is necessary. Without precise grid synchronization, our utilities' networks may face instability or black-out [5], [6].

Various power grid synchronization methods have been proposed in the literature [7]. In general, these prior-art synchronization approaches can be broken down into the following groups:

1) The first category is mathematical analysis approaches, mainly based on digital signal processing (DSP) techniques, which have strict requirements on the sampling rate [8].

2) The zero-crossing technique is more straightforward to realize and create; however, it is susceptible to voltage alterations of a power grid, especially for the harmonics and notches. Therefore, the reliability of the approach needs to be improved to meet the practical application [9].

3) Based on Phase-Locked Loop (PLL) technology, for balanced three-phase voltages, several approaches can detect the precise phase and frequency [10]–[13]. However, these methods face a potential instability issue in the converter and generator that may result from various reasons, such as PLL time delay, large harmonics, inaccurate modeling parameters, and severely unbalanced voltages.

Except for the methods mentioned above, recent advances in state estimation (SE) methods [14], which were first suggested in [15] and [16], are a key component of the grid synchronization technology. More importantly, recent advances in computing and phasor techniques have made it possible to use high-speed time-synchronization data captured by PMUs to do real-time dynamic estimates. Most of the published publications concentrated on measurement noise's effect on the accuracy

Manuscript received August 23, 2023; revised November 22, 2023; accepted December 2, 2023. Date of online publication February 14, 2024; date of current version March 20, 2024. This work was supported in part by the National Natural Science Foundation of China under Grant 62203395, in part by the Natural Science Foundation of Henan under Grant 242300421167, in part by the China Postdoctoral Science Foundation under Grant 2023TQ0306.

Y. Wang, Y. X. Liu, M. D. Wang (corresponding author, email: wangmingdong@zzu.edu.cn; ORCID: https://orcid.org/0000-0002-3292-2726) are with the School of Electrical and Information Engineering, Zhengzhou University, Zhengzhou 450001, China, and also with the Henan Engineering Research Center of Power Electronics and Energy Systems, Zhengzhou 450001, China.

V. Dinavahi is with the Department of Electrical and Computer Engineering, University of Alberta, Edmonton, AB T6G 2V4, Canada.

J. Liang is with the School of Engineering, Cardiff University, Cardiff CF24 3AA, UK.

Y. H. Sun is with the College of Energy and Electrical Engineering, Hohai University, Nanjing 210098, China.

DOI: 10.17775/CSEEJPES.2023.06900

of the grid synchronization estimation. Since measurement noise distribution is usually unknown and often deviates from the assumed Gaussian model, resulting in outliers, a robust estimation framework is designed in [17] to solve the unknown non-Gaussian noise and measurement time bias problems and obtain the optimal estimation. In reference [18], a CKF method based on generalized entropy loss (GCL) is proposed for complex non-Gaussian noise in power systems to improve the accuracy and flexibility of dynamic state estimation when there is bad measurement information. In reference [19], the concept of adaptive state estimation of power systems measured by PMU is proposed given the uncertainty and time-variability of measurement error characteristics. A Gaussian Laplacian mixed model is established to fit the unknown measurement error, and an adaptive estimation framework is proposed to generate more accurate state estimation.

However, it seldom concerns the impact of measurement data partial loss [20], [21]. As a result of sensor data dropouts in transmission channels of conventional measurements from meters to the control center, the missing data phenomenon constitutes one of the significant concerns in estimating power grid synchronization [22]–[24]. As noted in [25], the measurement signal from the sensor may include a damaged signal resulting from the potential sensor malfunction, which is not always correct. The sensor data loss may degrade the performance of conventional dynamic state estimators, which can severely distort the estimation results, resulting in entirely unreliable state estimates [26]–[28].

Some significant studies have been conducted in [29], [30] to deal with the issue of missing measurements. Most existing literature models missing measurements as a random variable obeying the Bernoulli distribution, with sensor data assumed to be either utterly missing or completely available. However, partial measurement missing is relatively common in practical applications, as it is rare for complete measurements to be lost [25]. For example, PMU data are converted from continuous measurement signals to digital data using analog-to-digital converters (ADCs). Poorly designed peripheral circuits or an unstable reference voltage can lead to fading output from ADCs [31]. It is important to remember that partially missing measurements differ significantly from lost measurement data, which was covered in the earlier study [32] and should be re-evaluated. *To the authors' knowledge, the power grid synchronization with partial missing measurements has not been thoroughly investigated. This also constitutes the main motivation of our current research.*

This paper aims to develop a novel resilient fault tolerant extended Kalman filter (RFTEKF), which can provide more reliable dynamic state estimation in power grid synchronization when partial measurements are missing. Compared to conventional EKFs, it can track power grid synchronization information more effectively. The main contributions of this paper are highlighted as follows:

- The estimation model of smart grid synchronization with partial measurement missing is established, where the time stamp technology is utilized to acquire the sensor data lost information.
- A novel resilient fault tolerant extended Kalman filter is proposed and derived, in which the gain is calculated using only the statistical characteristic of the lost information, where the randomness of partial missing is represented by a discrete distribution in the interval of [0, 1].
- Extensive simulation results show the efficiency of the proposed method and demonstrate that RFTEKF can provide more accurate results than conventional EKF and FTEKF.

Following is the remainder of this paper. First, the state space model for the smart grid synchronization with partial measurement missing is established in Section II. Then, Section II infers the conventional extended Kalman filter and the proposed resilient fault tolerant extended Kalman filter approach with specificity. Subsequently, to assess the effectiveness of the suggested approach, extensive simulations

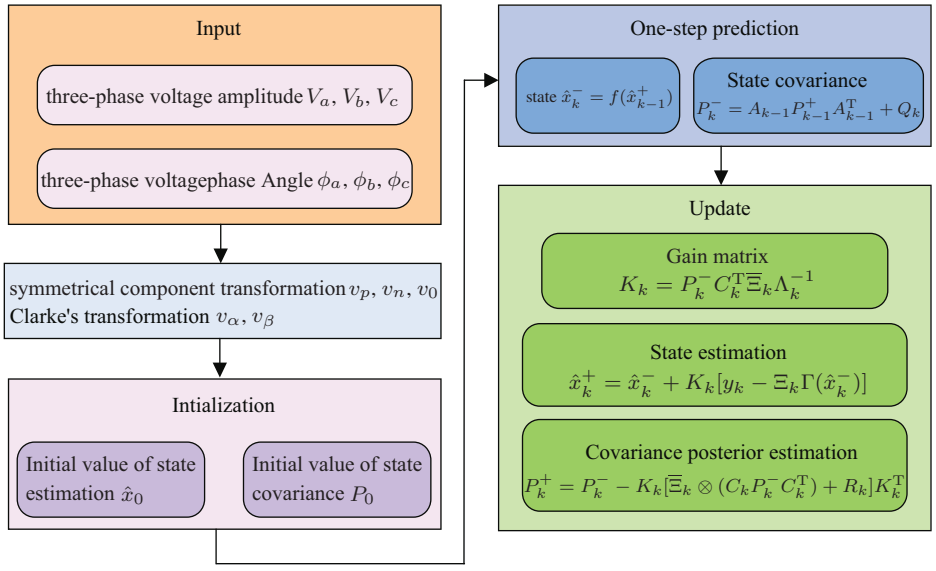

Fig. 1. Diagram of the proposed RFTEKF method.

are performed on various test systems, the estimation results are then provided, and finally, the conclusions are presented in Section V.

II. Problem Formulation

A. Basic Theory

In general, the general form of three-phase power system voltages can be expressed by:

$$\begin{cases} v_a(t) = \sqrt{2}V_a\cos(\omega t + \phi_a) \\ v_b(t) = \sqrt{2}V_b\cos(\omega t + \phi_b) \\ v_c(t) = \sqrt{2}V_c\cos(\omega t + \phi_c) \end{cases} \tag{1}$$

where $v_a(t), v_b(t), v_c(t)$ are the instantaneous unbalanced voltages of a, b, and c phases, respectively; t represents the time in seconds; ω indicates the electrical angular frequency in rad/s. $V_i (i = a, b, c)$ is the RMS voltage amplitudes, and ϕ_i is the corresponding RMS phase angles. Note that the voltage magnitudes of each phase are not necessarily equal, and the phase difference between each phase voltage might not be 120°.

From (1), the discrete three-phase voltages can be derived as:

$$\begin{cases} v_a(k) = \sqrt{2}V_a\cos(\omega kT + \phi_a) \\ v_b(k) = \sqrt{2}V_b\cos(\omega kT + \phi_b) \\ v_c(k) = \sqrt{2}V_c\cos(\omega kT + \phi_c) \end{cases} \tag{2}$$

where $k = 0, 1, 2, 3, \ldots$ represents the sampling instant. T is sampling period, $x(k) = x(kT)$ corresponds to the magnitude of $x(t)$ at the kth time instant. In general, the frequency of a power grid is considered to be 60 Hz, and the sampling frequency is 2400 Hz.

The variable $v(k) = [v_a(k), v_b(k), v_c(k)]^{\mathrm{T}}$ represents the three-phase voltage vector. According to the symmetrical component transformation, the unbalanced three-phase voltage can be represented as:

$$v(k) = v_0(k) + v_p(k) + v_n(k) \tag{3}$$

where $v(k)$ is the instantaneous three-phase voltage at time instant k; $v_p(k)$, $v_n(k)$ represent the positive, negative sequence voltages, respectively; $v_0(k)$ represents the zero sequence voltage:

$$\begin{cases} v_p(k) = \sqrt{2}V_p[\cos(\theta_p), \cos(\theta_p - 120°), \cos(\theta_p + 120°)]^{\mathrm{T}} \\ v_n(k) = \sqrt{2}V_n[\cos(\theta_n), \cos(\theta_n + 120°), \cos(\theta_n - 120°)]^{\mathrm{T}} \\ v_0(k) = \sqrt{2}V_0[\cos(\theta_0), \cos(\theta_0), \cos(\theta_0)]^{\mathrm{T}} \end{cases} \tag{4}$$

where $\theta_p, \theta_n, \theta_0$ are represent the positive, negative and zero sequence phase angles.

According to the symmetric component transformation, the three-phase voltage phasors under the abc coordinate frame can be separated into the zero, positive, and negative sequence phasors:

$$\begin{bmatrix} \overline{V}_a \\ \overline{V}_b \\ \overline{V}_c \end{bmatrix} = \begin{bmatrix} 1 & 1 & 1 \\ 1 & a^2 & a \\ 1 & a & a^2 \end{bmatrix} \begin{bmatrix} \overline{V}_0 \\ \overline{V}_p \\ \overline{V}_n \end{bmatrix} \tag{5}$$

where $a = 1\angle 120°$.

In addition, by using Clarke's transformation, the abc coordinate frame voltage phasors can be transformed into the voltage phasors of stationary $\alpha\beta$ coordinate frame:

$$\begin{bmatrix} \overline{V}_\alpha \\ \overline{V}_\beta \end{bmatrix} = \frac{2}{3}\begin{bmatrix} 1 & -\frac{1}{2} & -\frac{1}{2} \\ 0 & \frac{\sqrt{3}}{2} & -\frac{\sqrt{3}}{2} \end{bmatrix} \begin{bmatrix} \overline{V}_a \\ \overline{V}_b \\ \overline{V}_c \end{bmatrix} \tag{6}$$

By combining (5) and (6), the following can be derived:

$$\begin{bmatrix} \overline{V}_\alpha \\ \overline{V}_\beta \end{bmatrix} = \begin{bmatrix} 1 & 1 \\ -j & j \end{bmatrix} \begin{bmatrix} \overline{V}_p \\ \overline{V}_n \end{bmatrix} \tag{7}$$

Furthermore, voltage phasors $\overline{V}_\alpha$ and $\overline{V}_\beta$ can be discretized as $v_\alpha(k)$ and $v_\beta(k)$:

$$\begin{aligned} v_\alpha(k) &= \sqrt{2}V_p\cos(\omega kT + \phi_p) + \sqrt{2}V_n\cos(\omega kT + \phi_n) \\ &= \sqrt{2}(V_p\cos\phi_p + V_n\cos\phi_n)\cos\omega kT \\ &\quad - \sqrt{2}(V_p\sin\phi_p + V_n\sin\phi_n)\sin\omega kT \\ &= \sqrt{2}V_a\cos(\omega kT + \phi_\alpha) \end{aligned} \tag{8}$$

$$\begin{aligned} v_\beta(k) &= \sqrt{2}V_p\sin(\omega kT + \phi_p) - \sqrt{2}V_n\sin(\omega kT + \phi_n) \\ &= \sqrt{2}(V_p\cos\phi_p - V_n\cos\phi_n)\sin\omega kT \\ &\quad + \sqrt{2}(V_p\sin\phi_p - V_n\sin\phi_n)\cos\omega kT \\ &= \sqrt{2}V_\alpha\cos(\omega kT + \phi_\beta) \end{aligned} \tag{9}$$

Note after using Clarke's transformation, the zero sequence quantities in (7) are zeros.

B. Smart Grid Synchronization System Model

According to (8)–(9), the discrete grid synchronous voltage state space variables with sampling period T are chosen as follows:

$$\begin{cases} x_1(k) = \sqrt{2}V_\alpha\cos(k\omega T + \phi_\alpha) \\ x_2(k) = \sqrt{2}V_\alpha\sin(k\omega T + \phi_\alpha) \\ x_3(k) = \sqrt{2}V_\beta\cos(k\omega T + \phi_\beta) \\ x_4(k) = \sqrt{2}V_\beta\sin(k\omega T + \phi_\beta) \\ x_5(k) = \omega T \end{cases} \tag{10}$$

where $t = kT$ and $T = 1/f_s$, T and f_s are the sampling time and frequency, respectively.

According to (10), the smart grid synchronization system model can be formulated as follows:

$$\begin{cases} x_1(k+1) = x_1(k)\cos(x_5(k)) - x_2(k)\sin(x_5(k)) \\ x_2(k+1) = x_1(k)\sin(x_5(k)) + x_2(k)\cos(x_5(k)) \\ x_3(k+1) = x_3(k)\cos(x_5(k)) - x_4(k)\sin(x_5(k)) \\ x_4(k+1) = x_3(k)\sin(x_5(k)) + x_4(k)\cos(x_5(k)) \\ x_5(k+1) = x_5(k) \end{cases} \tag{11}$$

The process noise in (11) is usually considered to be zero. The measurement functions are expressed as:

$$\begin{aligned} \boldsymbol{z}_1(k) &= x_1(k) + \zeta_1(k) \\ \boldsymbol{z}_2(k) &= x_3(k) + \zeta_2(k) \end{aligned} \tag{12}$$

where $\zeta_1(k)$ and $\zeta_2(k)$ are deemed to be external disturbances.

C. Calculation of Positive Sequence Voltage

At first, by taking the invert the matrix in (7), the following equation can be derived:

$$\begin{bmatrix}\overline{V}_p\\ \overline{V}_n\end{bmatrix}=\frac{1}{2}\begin{bmatrix}1 & j\\ 1 & -j\end{bmatrix}\begin{bmatrix}\overline{V}_\alpha\\ \overline{V}_\beta\end{bmatrix} \tag{13}$$

Then, based on Euler's formula, the positive voltage vector can be derived by expanding the first row of the matrix (13):

$$\begin{aligned}\overline{V}_p = V_p\angle\theta_p &= \frac{1}{2}(\overline{V}_\alpha + j\overline{V}_\beta)\\ &= 0.5[(V_\alpha\cos\theta_\alpha - V_\beta\sin\theta_\beta)\\ &\quad + j(V_\alpha\sin\theta_\alpha + V_\beta\cos\theta_\beta)]\end{aligned} \tag{14}$$

Thus, the magnitude and phase angle of positive sequence voltage can be acquired as follows [32]:

$$\theta_p = \tan^{-1}\frac{V_\alpha\sin(\theta_\alpha)+V_\beta\cos(\theta_\beta)}{V_\alpha\cos(\theta_\alpha)-V_\beta\sin(\theta_\beta)} \tag{15}$$

$$V_p = \frac{1}{2}\sqrt{(V_\alpha\sin\theta_\alpha+V_\beta\cos\theta_\beta)^2+(V_\alpha\cos\theta_\alpha-V_\beta\sin\theta_\beta)^2} \tag{16}$$

D. Smart Grid Synchronization System Model with Partial Missing Measurements

Based on the smart grid synchronization system model described by (11)–(12), the discrete power grid system process and measurement equations with partial missing measurements can be expressed by:

$$\begin{cases}\boldsymbol{x}_{k+1} = \boldsymbol{f}(\boldsymbol{x}_k)+\boldsymbol{v}_k\\ \boldsymbol{y}_k = \begin{pmatrix}\gamma_k^1\boldsymbol{\Gamma}^1(\boldsymbol{x}_k)+\boldsymbol{\varsigma}_k^1\\ \gamma_k^2\boldsymbol{\Gamma}^2(\boldsymbol{x}_k)+\boldsymbol{\varsigma}_k^2\\ \vdots\\ \gamma_k^m\boldsymbol{\Gamma}^m(\boldsymbol{x}_k)+\boldsymbol{\varsigma}_k^m\end{pmatrix} = \boldsymbol{\Xi}_k\boldsymbol{\Gamma}(\boldsymbol{x}_k)+\boldsymbol{\varsigma}_k\end{cases} \tag{17}$$

where $\boldsymbol{x}_k \in \boldsymbol{R}^n$ - state variable; $\boldsymbol{y}_k \in \boldsymbol{R}^m$ - measurement vector with partial measurements missing; $\boldsymbol{f}, \boldsymbol{\Gamma}$ - system and measurement functions; $\boldsymbol{v}_k, \boldsymbol{\varsigma}_k$ - process noise and measurement noise are commonly depicted as zero-mean Gaussian white noises with covariance matrices Q_k and R_k, respectively.

In addition, $\boldsymbol{\Xi}_k = \mathrm{diag}\{\gamma_k^1, \gamma_k^2, \cdots \gamma_k^m\}$ and $\boldsymbol{\gamma}_k^i (i = 1, 2, \cdots, m)$ are m independent random variables, which are independent of the system noise and measurement noise. Where $\boldsymbol{\Gamma}(\boldsymbol{x}_k) = \mathrm{diag}\{\Gamma^1(x_k), \Gamma^2(x_k), \cdots \Gamma^m(x_k)\}$, and the random variable $\gamma_{m,k}$ represents the mth measurement partial loss coefficient, which obeys uniform distribution of [0, 1] interval.

III. Proposed Resilient Fault Tolerant Extended Kalman Filter

In this section, as an essential theoretical basis, the main implementation framework of the conventional extended Kalman filter method is first introduced briefly. Then, a novel resilient fault-tolerant extended Kalman filter is developed and proved to acquire a more reliable dynamic state estimation that can deal with the issue of partial missing measurements in the PMU-based power grid synchronization.

Some basic theories and necessary lemmas will be introduced to facilitate deriving a resilient fault-tolerant extended Kalman filter approach.

Lemma 1 [33]: Given two matrices $\boldsymbol{A}_{m\times n}$ and $\boldsymbol{B}_{n\times n}$, where $\boldsymbol{B}_{n\times n} = \boldsymbol{B}_{n\times n}^{\mathrm{T}}$, then the partial derivative of $\mathrm{tr}(\boldsymbol{ABA}^{\mathrm{T}})$, with respect to A, can be derived as follows:

$$\frac{\partial\,\mathrm{tr}(\boldsymbol{ABA}^{\mathrm{T}})}{\partial\boldsymbol{A}} = 2\boldsymbol{AB} \tag{18}$$

where $\mathrm{tr}(\cdot)$ represents the trace of the matrix.

Lemma 2 [34]: Given a real-valued matrix $\boldsymbol{A} = [a_{ij}]_{p\times p}$ and a diagonal stochastic matrix $\boldsymbol{B} = \mathrm{diag}(b_1, b_2, \cdots b_p)$, then

$$E(\boldsymbol{BAB}^{\mathrm{T}}) = \begin{bmatrix}E(b_1^2)E(b_1b_2)\cdots E(b_1b_p)\\ E(b_1b_2)E(b_2^2)\cdots E(b_2b_p)\\ \cdots\\ E(b_pb_1)E(b_pb_2)\cdots E(b_p^2)\end{bmatrix}\otimes\boldsymbol{A} \tag{19}$$

where $E(\cdot)$ is the mathematical expectation, $\otimes$ represents the Hadamard product.

For convenience, $\hat{x}_k^-$ denotes the a prior estimator of x_k, $\hat{x}_k^+$ represents the posteriori estimate of x_k, which are expressed as follows:

$$\begin{cases}\hat{\boldsymbol{x}}_k^- = E[\boldsymbol{x}_k|\boldsymbol{y}_1, \boldsymbol{y}_2, \cdots \boldsymbol{y}_{k-1}]\\ \hat{\boldsymbol{x}}_k^+ = E[\boldsymbol{x}_k|\boldsymbol{y}_1, \boldsymbol{y}_2, \cdots \boldsymbol{y}_k]\end{cases} \tag{20}$$

A. Extended Kalman Filter

As a conventional nonlinear dynamic state estimator, EKF has been widely used in state estimation and parameter identification of nonlinear systems [35], [36].

In general, the recursive form of EKF can be summarized as follows:

$$\hat{\boldsymbol{x}}_{k+1}^- = \boldsymbol{f}(\hat{\boldsymbol{x}}_k^+) \tag{21}$$

$$\hat{\boldsymbol{x}}_{k+1}^+ = \hat{\boldsymbol{x}}_{k+1}^- + \boldsymbol{K}_{k+1}[\boldsymbol{y}_{k+1} - \boldsymbol{\Gamma}(\hat{\boldsymbol{x}}_{k+1}^-)] \tag{22}$$

Let $\boldsymbol{e}_{k+1}^- = \boldsymbol{x}_{k+1} - \hat{\boldsymbol{x}}_{k+1}^-$ represent the a priori state estimation errors and $\boldsymbol{e}_{k+1}^+ = \boldsymbol{x}_{k+1} - \hat{\boldsymbol{x}}_{k+1}^+$ indicate the posteriori state estimation errors of the system, respectively. Then, we can get:

$$\boldsymbol{P}_{k+1}^- = \boldsymbol{E}(\boldsymbol{e}_{k+1}^-(\boldsymbol{e}_{k+1}^-)^{\mathrm{T}}) \tag{23}$$

$$\boldsymbol{P}_{k+1}^+ = \boldsymbol{E}(\boldsymbol{e}_{k+1}^+(\boldsymbol{e}_{k+1}^+)^{\mathrm{T}}) \tag{24}$$

The standard EKF is of the following form:

1) Initialization

$$\hat{\boldsymbol{x}}_0 = E(\boldsymbol{x}_0) \tag{25}$$

$$\boldsymbol{P}_0 = E[(\boldsymbol{x}_0 - \hat{\boldsymbol{x}}_0)(\boldsymbol{x}_0 - \hat{\boldsymbol{x}}_0)^{\mathrm{T}}] \tag{26}$$

2) State Prediction

a) Calculation of Jacobian matrices

$$\boldsymbol{A}_k = \left.\frac{\partial\boldsymbol{f}(\boldsymbol{x}_k, \boldsymbol{u}_k)}{\partial\boldsymbol{x}_k}\right|_{\boldsymbol{x}_k=\hat{\boldsymbol{x}}_k^+} \tag{27}$$

b) Time update equation

$$\hat{\boldsymbol{x}}_k^- = \boldsymbol{f}(\hat{\boldsymbol{x}}_{k-1}^+) \tag{28}$$

$$\boldsymbol{P}_k^- = \boldsymbol{A}_{k-1}\boldsymbol{P}_{k-1}^+\boldsymbol{A}_{k-1}^{\mathrm{T}} + \boldsymbol{Q}_k \tag{29}$$

3) State Update

a) Computation of Jacobian matrices

$$\boldsymbol{C}_k = \left.\frac{\partial \boldsymbol{\Gamma}(\boldsymbol{x}_k)}{\partial \boldsymbol{x}_k}\right|_{\boldsymbol{x}_k=\hat{\boldsymbol{x}}_k^-} \tag{30}$$

b) Computation of the Kalman gain at time instant k

$$\boldsymbol{K}_k = \boldsymbol{P}_k^- \boldsymbol{C}_k^{\mathrm{T}} \times (\boldsymbol{C}_k \boldsymbol{P}_k^- \boldsymbol{C}_k^{\mathrm{T}} + \boldsymbol{R}_k)^{-1} \tag{31}$$

c) Update of the posterior state estimate at the time of instant k

$$\hat{\boldsymbol{x}}_k^+ = \hat{\boldsymbol{x}}_k^- + \boldsymbol{K}_k[\boldsymbol{y}_k - \boldsymbol{\Gamma}(\hat{\boldsymbol{x}}_k^-)] \tag{32}$$

d) Update of state estimation error covariance at the time instant k

$$\boldsymbol{P}_k^+ = (\boldsymbol{I} - \boldsymbol{K}_k \boldsymbol{C}_k)\boldsymbol{P}_k^- \tag{33}$$

Remark 1: Due to the characteristics of simple calculation and high efficiency, the conventional extended Kalman filter has been widely utilized in many areas, such as dynamic state estimation of power systems, vehicle state estimation, and state estimation of lithium batteries [37], [38]. The standard EKF method can work well if the measurement data acquired are correct. However, these assumptions are difficult to hold due to sensor data dropouts inevitably occurring in the transmission channels of conventional measurements from the meters to the control center. The sensor data loss may degrade the performance of conventional EKF, which can severely distort its estimation results, resulting in unreliable state estimates.

B. Resilient Fault Tolerant Extended Kalman Filter

In this subsection, a resilient, dynamic estimation method for smart power grid synchronization is developed to acquire a more reliable and accurate result of power grid synchronization, which could mitigate the adverse effect of inevitably partial sensor data loss, named resilient fault tolerant extended Kalman filter.

Considering partial measurements of the smart grid synchronization system in (17) are missing, if all the conditions in (34) are satisfied:

$$\begin{cases} E[\boldsymbol{v}_k] = 0,\ E[\boldsymbol{\varsigma}_k] = 0,\ E[\boldsymbol{v}_k \boldsymbol{\varsigma}_j^{\mathrm{T}}] = 0 \\ E[\boldsymbol{v}_k \boldsymbol{v}_j^{\mathrm{T}}] = \boldsymbol{Q}_k \boldsymbol{\Omega}_{k-j},\ E[\boldsymbol{\varsigma}_k \boldsymbol{\varsigma}_j^{\mathrm{T}}] = \boldsymbol{R}_k \boldsymbol{\Omega}_{k-j} \\ \boldsymbol{\Omega}_{k-j} = 1(k=j);\ \boldsymbol{\Omega}_{k-j} = 0(k \neq j) \\ E[\boldsymbol{v}_k \boldsymbol{x}_0^{\mathrm{T}}] = 0,\ E[\boldsymbol{\varsigma}_k \boldsymbol{x}_0^{\mathrm{T}}] = 0 \end{cases} \tag{34}$$

Then, the RFTEKF method can be derived for grid synchronization DSE with partial missing measurements.

Based on the DSE model of power grid synchronization described in (17), the RFTEKF method can be further constructed as:

$$\hat{\boldsymbol{x}}_{k+1}^- = \boldsymbol{f}(\hat{\boldsymbol{x}}_k^+) \tag{35}$$

$$\hat{\boldsymbol{x}}_{k+1}^+ = \hat{\boldsymbol{x}}_{k+1}^- + \boldsymbol{K}_{k+1}[\boldsymbol{y}_{k+1} - \boldsymbol{\Xi}_{k+1}\boldsymbol{\Gamma}(\hat{\boldsymbol{x}}_{k+1}^-)] \tag{36}$$

where $\boldsymbol{\Xi}$ is used to describe the partial missing measurements. To express convenience, we define $\boldsymbol{\varepsilon}_k \triangleq \boldsymbol{y}_k - \boldsymbol{\Xi}_k \boldsymbol{\Gamma}(\hat{\boldsymbol{x}}_k^-)$.

Then, the optimal filter gain of RFTEKF can be derived as follows:

$$\boldsymbol{K}_{k+1} = \boldsymbol{P}_{k+1}^- \boldsymbol{C}_{k+1}^{\mathrm{T}} \overline{\boldsymbol{\Xi}}_{k+1} \boldsymbol{\Lambda}_{k+1}^{-1} \tag{37}$$

where $\boldsymbol{\Lambda}_{k+1} = \overline{\boldsymbol{\Xi}}_{k+1} \otimes (\boldsymbol{C}_{k+1} \boldsymbol{P}_{k+1}^- \boldsymbol{C}_{k+1}^{\mathrm{T}}) + \boldsymbol{R}_{k+1}$ and $\overline{\boldsymbol{\Xi}}_{k+1} = E(\boldsymbol{\Xi}_{k+1})$.

$\boldsymbol{P}_{k+1}^+$ can be written as:

$$\boldsymbol{P}_{k+1}^+ = \boldsymbol{P}_{k+1}^- - \boldsymbol{K}_{k+1} \boldsymbol{\Lambda}_{k+1} \boldsymbol{K}_{k+1}^{\mathrm{T}} \tag{38}$$

Proof: Let

$$\begin{cases} \boldsymbol{e}_{k+1}^+ = \boldsymbol{x}_{k+1} - \hat{\boldsymbol{x}}_{k+1}^+ \\ \boldsymbol{e}_{k+1}^- = \boldsymbol{x}_{k+1} - \hat{\boldsymbol{x}}_{k+1}^- \end{cases} \tag{39}$$

where $\boldsymbol{e}_{k+1}^+$ represents the state estimation error, $\boldsymbol{e}_{k+1}^-$ indicates the prior state prediction error. According to (35), $\boldsymbol{e}_{k+1}^+$ and $\boldsymbol{e}_{k+1}^-$ can be further rewritten as follows:

$$\boldsymbol{e}_{k+1}^+ = \boldsymbol{f}(\boldsymbol{x}_k) + \boldsymbol{v}_k - \hat{\boldsymbol{x}}_{k+1}^- - \boldsymbol{K}_{k+1}\varepsilon_{k+1} \tag{40}$$

$$\boldsymbol{e}_{k+1}^- = \boldsymbol{f}(\boldsymbol{x}_k) + \boldsymbol{v}_k - \boldsymbol{f}(\hat{\boldsymbol{x}}_k^+) \tag{41}$$

Taylor expansion is used to linearize $\boldsymbol{f}(\boldsymbol{x}_k)$ and $\boldsymbol{\Gamma}(\boldsymbol{x}_{k+1})$ at $\hat{\boldsymbol{x}}_k^+$ and $\hat{\boldsymbol{x}}_{k+1}^-$, respectively, and leaving only the first-order term:

$$\begin{cases} \boldsymbol{f}(\boldsymbol{x}_k) = \boldsymbol{f}(\hat{\boldsymbol{x}}_k^+) + \boldsymbol{A}_k \boldsymbol{e}_k^+ \\ \boldsymbol{A}_k = \left.\dfrac{\partial \boldsymbol{f}(\boldsymbol{x}_k)}{\partial \boldsymbol{x}_k}\right|_{\boldsymbol{x}_k=\hat{\boldsymbol{x}}_k^+} \end{cases} \tag{42}$$

$$\boldsymbol{e}_{k+1}^- = \boldsymbol{A}_k \boldsymbol{e}_k^+ + \boldsymbol{v}_k \tag{43}$$

$$\begin{cases} \boldsymbol{\Gamma}(\boldsymbol{x}_{k+1}) = \boldsymbol{\Gamma}(\hat{\boldsymbol{x}}_{k+1}^-) + \boldsymbol{C}_{k+1} \boldsymbol{e}_{k+1}^- \\ \boldsymbol{C}_{k+1} = \left.\dfrac{\partial \boldsymbol{\Gamma}(\boldsymbol{x}_{k+1})}{\partial \boldsymbol{x}_{k+1}}\right|_{\boldsymbol{x}_{k+1}=\hat{\boldsymbol{x}}_{k+1}^-} \end{cases} \tag{44}$$

$$\boldsymbol{e}_{k+1}^+ = (\boldsymbol{I} - \boldsymbol{K}_{k+1} \boldsymbol{\Xi}_{k+1} \boldsymbol{C}_{k+1}) \boldsymbol{e}_{k+1}^- - \boldsymbol{K}_{k+1} \varsigma_{k+1} \tag{45}$$

According to the (37), $\boldsymbol{P}_{k+1}^-$ can be computed by

$$\boldsymbol{P}_{k+1}^- = \boldsymbol{E}[\boldsymbol{e}_{k+1}^- (\boldsymbol{e}_{k+1}^-)^{\mathrm{T}}] = \boldsymbol{A}_k \boldsymbol{P}_k^+ \boldsymbol{A}_k^{\mathrm{T}} + \boldsymbol{Q}_k \tag{46}$$

Due to $\boldsymbol{v}_k$, $\boldsymbol{e}_k$, $\boldsymbol{\varsigma}_k$ and $\overline{\boldsymbol{\Xi}}_k$ are mutually uncorrelated, according to (39), $\boldsymbol{P}_{k+1}^+$ is generated as follows:

$$\begin{aligned} \boldsymbol{P}_{k+1}^+ &= \boldsymbol{E}[\boldsymbol{e}_{k+1}^+ (\boldsymbol{e}_{k+1}^+)^{\mathrm{T}}] \\ &= \boldsymbol{P}_{k+1}^- - \boldsymbol{P}_{k+1}^- \boldsymbol{C}_{k+1}^{\mathrm{T}} \overline{\boldsymbol{\Xi}}_{k+1} \boldsymbol{K}_{k+1}^{\mathrm{T}} \\ &\quad - \boldsymbol{K}_{k+1} \overline{\boldsymbol{\Xi}}_{k+1} \boldsymbol{C}_{k+1} (\boldsymbol{P}_{k+1}^-)^{\mathrm{T}} \\ &\quad + (\boldsymbol{K}_{k+1} - \boldsymbol{K}_{k+1}^*) \boldsymbol{\Lambda}_{k+1} (\boldsymbol{K}_{k+1} - \boldsymbol{K}_{k+1}^*)^{\mathrm{T}} \\ &\quad - \boldsymbol{K}_{k+1}^* \boldsymbol{\Lambda}_{k+1} (\boldsymbol{K}_{k+1}^*)^{\mathrm{T}} + \boldsymbol{K}_{k+1}^* \boldsymbol{\Lambda}_{k+1} \boldsymbol{K}_{k+1}^{\mathrm{T}} \\ &\quad + \boldsymbol{K}_{k+1} \boldsymbol{\Lambda}_{k+1} (\boldsymbol{K}_{k+1}^*)^{\mathrm{T}} \end{aligned} \tag{47}$$

When $\boldsymbol{K}_{k+1} = \boldsymbol{K}_{k+1}^* = \boldsymbol{P}_{k+1}^- \boldsymbol{C}_{k+1}^{\mathrm{T}} \overline{\boldsymbol{\Xi}}_{k+1} \boldsymbol{\Lambda}_{k+1}^{-1}$, $\boldsymbol{P}_{k+1}^+$ can acquire minimum value. Thus, $\boldsymbol{P}_{k+1}^+$ and $\boldsymbol{K}_{k+1}$ can be written as:

$$\begin{cases} \boldsymbol{P}_{k+1}^+ = \boldsymbol{P}_{k+1}^- - \boldsymbol{K}_{k+1} \boldsymbol{\Lambda}_{k+1} \boldsymbol{K}_{k+1}^{\mathrm{T}} \\ \boldsymbol{K}_{k+1} = \boldsymbol{P}_{k+1}^- \boldsymbol{C}_{k+1}^{\mathrm{T}} \overline{\boldsymbol{\Xi}}_{k+1} \boldsymbol{\Lambda}_{k+1}^{-1} \end{cases} \tag{48}$$

This completes the proof.

At last, for simplicity, Algorithm 1 is a summary of the proposed RFTEKF method.

Remark 2: When designing the estimator, literature [35] only adopted the statistical property of measurement data loss in formula (18) to improve the calculation accuracy. However, when referring to the design and implementation of the estimator in [39], the time stamp technology in the sensor network

Algorithm 1: Resilient Fault Extended Kalman Filter Method

Step 1: set $k=0$, $\hat{\boldsymbol{x}}_0, \boldsymbol{P}_0, T_s$;

Step 2: calculate $\hat{\boldsymbol{x}}_k^-$ at time instant k by (35)

$$\hat{\boldsymbol{x}}_k^- \leftarrow \boldsymbol{f}(\hat{\boldsymbol{x}}_{k-1}^+);$$

Step 3: calculate $\boldsymbol{P}_k^-$ at the time instant k by (46)

$$\boldsymbol{P}_k^- = \boldsymbol{A}_{k-1}\boldsymbol{P}_{k-1}^+\boldsymbol{A}_{k-1}^{\mathrm{T}} + \boldsymbol{Q}_k;$$

Step 4: update the gain matrix $\boldsymbol{K}_k$ at the time instant k by (37)

$$\boldsymbol{K}_{k+1} = \boldsymbol{P}_{k+1}^-\boldsymbol{C}_{k+1}^{\mathrm{T}}\overline{\boldsymbol{\Xi}}_{k+1}\boldsymbol{\Lambda}_{k+1}^{-1}$$

Step 5: update the estimated state vector $\hat{\boldsymbol{x}}_k^+$ by (36)

$$\hat{\boldsymbol{x}}_k^+ = \hat{\boldsymbol{x}}_k^- + \boldsymbol{K}_k[\boldsymbol{y}_k - \boldsymbol{\Xi}_k\boldsymbol{\Gamma}(\hat{\boldsymbol{x}}_k^-)];$$

Step 6: update the estimation covariance matrix $\boldsymbol{P}_k^+$ by (38)

$$\boldsymbol{P}_k^+ = \boldsymbol{P}_k^- - \boldsymbol{K}_k[\overline{\boldsymbol{\Xi}}_k \otimes (\boldsymbol{C}_k\boldsymbol{P}_k^-\boldsymbol{C}_k^{\mathrm{T}}) + \boldsymbol{R}_k]\boldsymbol{K}_k^{\mathrm{T}};$$

Step 7: output the state estimation results of $\hat{\boldsymbol{x}}_k$, and update the time instant

Step 8: $k = k+1$, go back to *Step 2*

until $k = T_s$, end loop

can be used to know Ξ. In this literature, similar to [40], only Ξ statistical characteristics are used to construct the best possible filter gains for the RFTEKF. More importantly, using one Riccati, the gains can be computed offline [39]. Meanwhile, the timestamp mechanism implements the RFTEKF approach to assume Ξ is known online.

IV. Simulation Results and Analysis

Detailed numerical simulations are implemented in this section to show the effectiveness and resistance of the proposed resilient fault-tolerant extended Kalman filter against partial missing measurements.

A. Test Systems

To verify the validity and robustness of the proposed method, numerical signal analysis, WECC 9-bus test and real power system with DPGS test are carried out. The following are the precise settings for each testing system.

Case Study 1: The proposed RFTEKF method is compared with FTEKF and conventional extended Kalman filter for the numerical signal with partial missing measurement.

Case Study 2: To further illustrate the effectiveness of the developed RFTEKF method, the discussed approaches are tested on the three-phase voltage imbalance signal acquired between bus 8 and bus 9 of the standard WECC 9-bus test system.

Case Study 3: To verify the effectiveness of the proposed method in a large power system with a high proportion of new energy access, a signal from the actual power system with DPGS penetration in Henan Province, China, is considered and tested further to demonstrate the scalability and effectiveness of the method.

To accurately track the dynamic features of the smart grid, in this paper, the time step for the simulation is set at 0.25 seconds. The sampling frequency is selected as 2400 Hz. It's important to note each of the discussed approaches is carried out in MATLAB R2020b on a PC with the Intel Core CPU i5-7200U, 2.5 GHz and 8 GB RAM.

In addition, to obtain more comprehensive and substantial results and to make the statistical results clearer and easier to understand, the overall performance indicator E_x introduced in the revised manuscript to evaluate the performance of each discussed algorithm with the 100 Monte Carlo simulations conducted, which is defined as follows:

$$E_x = \frac{1}{N_{MC}}\sum_{i=1}^{N_{MC}}\sqrt{\sum_{k=1}^{N_T}(\hat{x}_k - x_k)^2/N_T} \tag{49}$$

where $N_{MC}=100$ is the number of Monte Carlo runs; N_T is the simulation time steps k represents the time instant, $\boldsymbol{x}$ denotes the magnitude and phase angle of positive sequence voltage, $\hat{\boldsymbol{x}}_k$ and $\boldsymbol{x}_k$ are the estimated value and the truth value of the state variable, respectively.

B. Case Study 1: Numerical Signal Test

In this part, the numerical simulation of the three-phase unbalanced voltage signal is carried out. The performance of traditional EKF, FTEKF and the proposed RFTEKF are tested. In the simulation studies, the initial value of the amplitude of the unbalanced voltage is set $[1, 1.2, 0.8]^{\mathrm{T}}$, and the initial value of the phase angle is selected as $[0°, 120°, 240°]^{\mathrm{T}}$.

In the simulation, the sampling frequency is 2400 Hz. The initial value of the error covariance of the EKF, FTEKF and RFTEKF is chosen as $10^{-6}\boldsymbol{I}_{n\times n}$. The system and measurement noise covariance matrices are set as $\boldsymbol{Q}_0 = 10^{-6}\boldsymbol{I}_{5\times 5}, \boldsymbol{R}_0 = 10^{-6}\boldsymbol{I}_{2\times 2}$, respectively.

Figures 2 and 3 show the complete measurement information of $\boldsymbol{y}_1$ and $\boldsymbol{y}_2$ with and without partial missing measurements. Based on which, we have compared traditional EKF, FTEKF and proposed RFTEKF three methods state estimation tests for power grid synchronization. The comparison results of the discussed approaches are presented in Figs. 4–8.

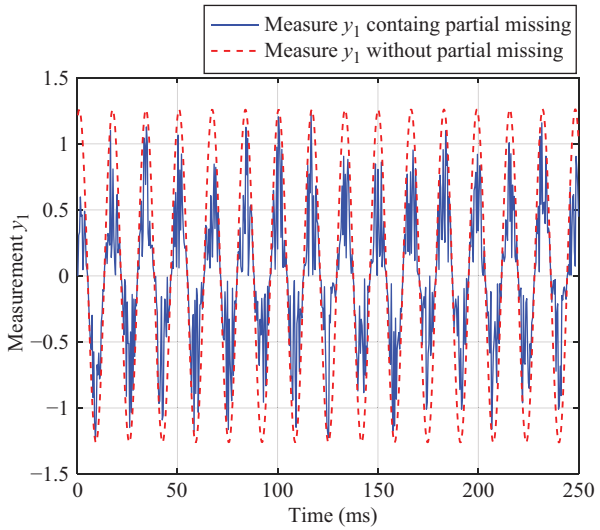

Fig. 2. Measurement $\boldsymbol{y}_1$ with and without partial missing.

As a result of the experimental findings, it can be seen that the proposed resilient fault-tolerant extended Kalman filter

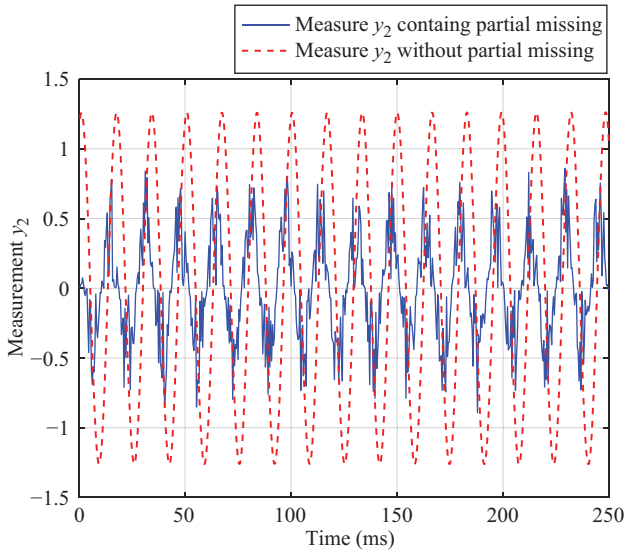

Fig. 3. Measurement $\boldsymbol{y}_2$ with and without partial missing.

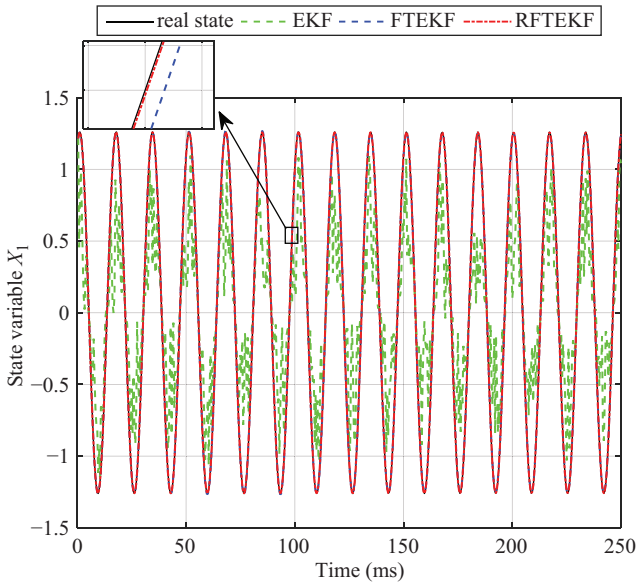

Fig. 4. Estimation results of state variables $\boldsymbol{x}_1$ by different methods.

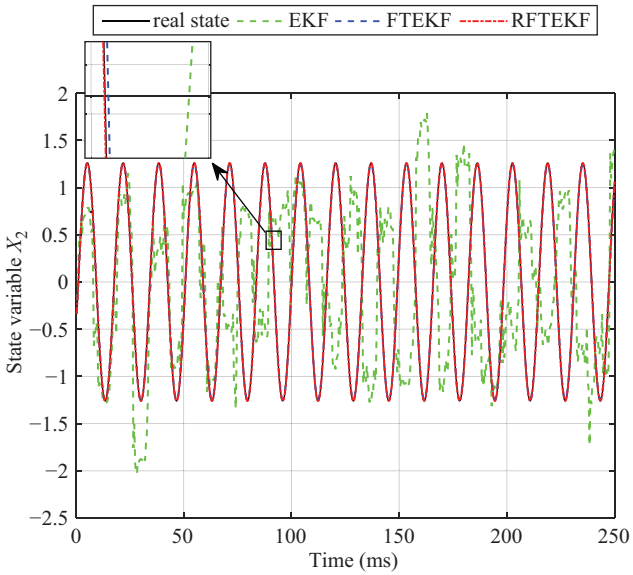

Fig. 5. Estimation results of state variables $\boldsymbol{x}_2$ by different methods.

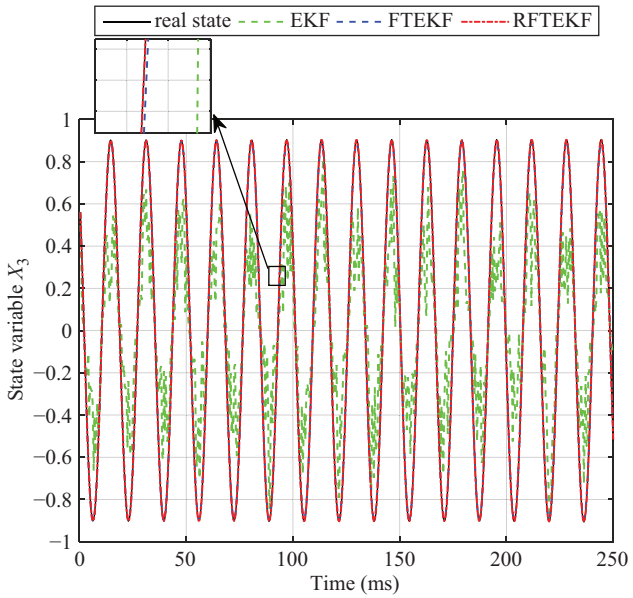

Fig. 6. Estimation results of state variables $\boldsymbol{x}_3$ by different methods.

approach can accurately estimate each state variable, even with partial missing measurements. FTEKF is second because it only considers the statistical properties of lost information. Due to the severe nonlinearity caused by the partial missing measurement, the conventional extended Kalman filter significantly deviates from the true value. It cannot converge to the real values of the five state trajectories. In the case of sensor data loss, the conventional EKF method exhibits numerical instability because the EKF methodology uses first-order linearization to update the estimation covariance matrix and mean state.

Additionally, Table I summarizes the performance indices of EKF, FTEKF and the proposed RFTEKF methods for power grid synchronization with partial missing measurements. It can be seen that compared to the traditional EKF method and FTEKF, the estimation error of the new RFETKF methodology is significantly lower. These experimental outcomes are consistent with those reflected in Figs. 4–8 further verifies and confirms that the proposed RFTEKF approach is more robust and resistant to measurements with partly missing data.

TABLE I
PERFORMANCE COMPARISON

Metric	EKF	FTEKF	RFTEKF
E_{X_1}	0.0498	0.0111	0.0003
E_{X_2}	1.2820	0.0478	0.0050
E_{X_3}	0.3469	0.0096	0.0024
E_{X_4}	0.8864	0.0122	0.0043
E_{X_5}	0.2490	0.0088	0.0019

C. Case Study 2: WECC 9-Bus Test

In this scenario, the 3-machine and 9-bus system of the

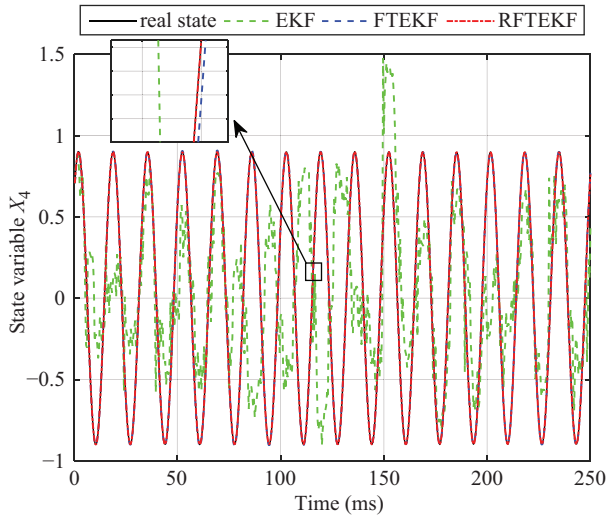

Fig. 7. Estimation results of state variables $\boldsymbol{x}_4$ by different methods.

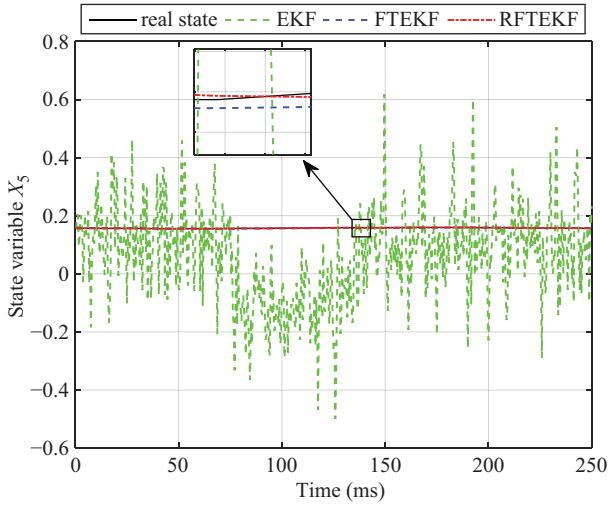

Fig. 8. Estimation results of state variables $\boldsymbol{x}_5$ by different methods.

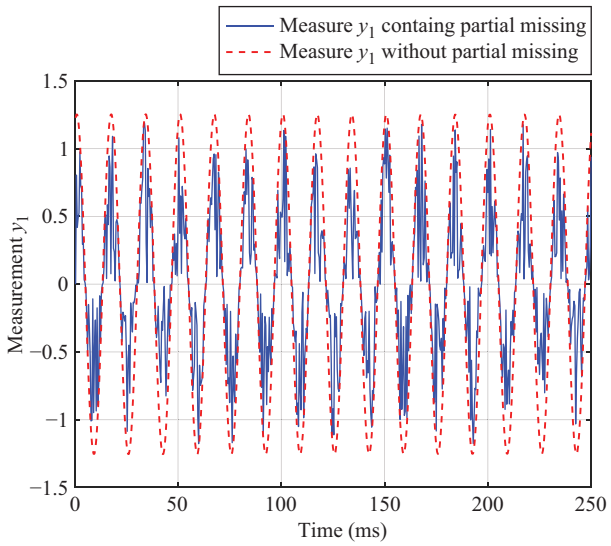

Fig. 9. Measurement $\boldsymbol{y}_1$ with and without partial missing.

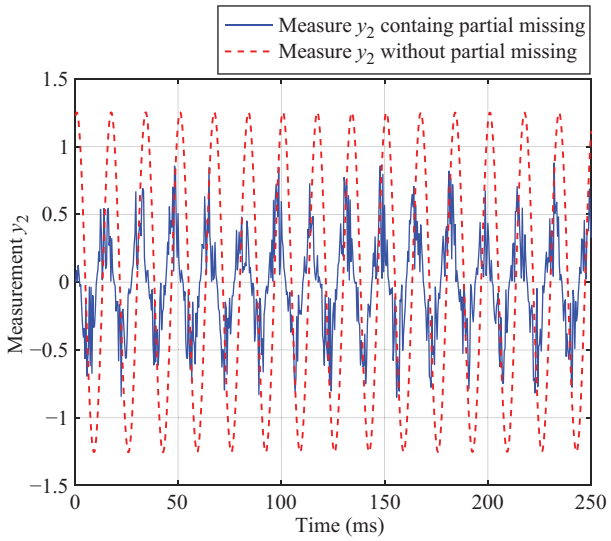

Fig. 10. Measurement $\boldsymbol{y}_2$ with and without partial missing.

Western Electric Power Coordinating Committee (WECC) is selected as the test system [31]. The unbalanced voltage signal is acquired between bus 8 and bus 9 of the test system. The measurement data with partial missing are displayed in Figs. 9–10. Three-phase unbalanced voltage's initial amplitude and phase angle are $[1, 1.11, 0.89]^{\mathrm{T}}$ and $[0°, 120.33°, 240.32°]^{\mathrm{T}}$, respectively. In addition, $10^{-6}\boldsymbol{I}_{n\times n}$ is selected as the initial value of the error covariance of the EKF and RFTEKF. The system noise covariance matrix is $\boldsymbol{Q}_0 = 10^{-6}\boldsymbol{I}_{5\times5}$ and the measurement noise covariance matrix is $\boldsymbol{R}_0 = 10^{-6}\boldsymbol{I}_{5\times5}$.

The conventional EKF, FTEKF and RFTEKF approaches are implemented for dynamic state estimation of WECC synchronization. The estimation outcomes based on EKF, FTEKF and RFTEKF are contrasted with actual values of state variables, which are displayed in Figs. 11–15.

According to the experimental findings shown in Figs. 11–15, the synchronization estimation of traditional EKF deviates from true value seriously under this scenario, which reflects conventional EKF is susceptible to partial missing measurement. FTEKF performs better than EKF because the estimator is designed with measurement missing in mind. The developed RFTEKF method, in contrast, outperforms the traditional EKF method and FTEKF in accurately tracking the dynamic of the WECC system, even with partial missing measurements. These results demonstrate the excellent performance and numerical stability of the proposed RFTEKF method in the case of the partial missing measurement.

In addition, to acquire a quantitative understanding of the performance comparison of each discussed approach, Table II provides an overview of the estimation error index for the proposed RFTEKF, FTEKF and EKF methods for the WECC test. It is evident from the table the proposed RFTEKF method can achieve a much smaller root-mean-square error than the conventional EKF. These experimental findings concur with Case Study 2, which shows the RFTEKF method is more resilient and robust when dealing with partial missing measurements.

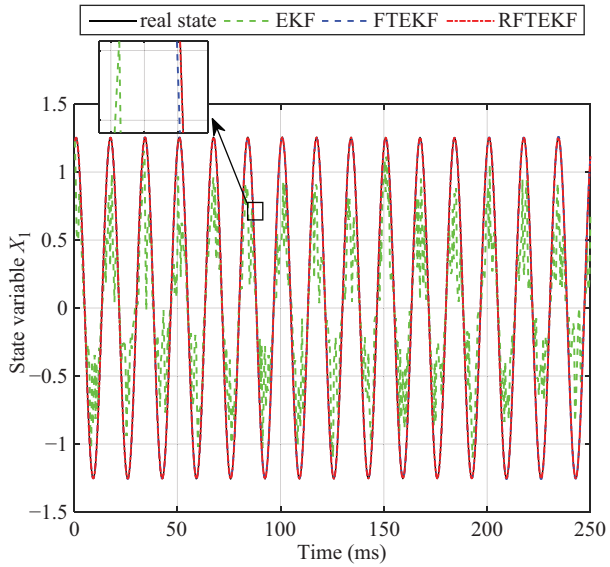

Fig. 11. Estimation results of state variables $\boldsymbol{x}_1$ by different methods.

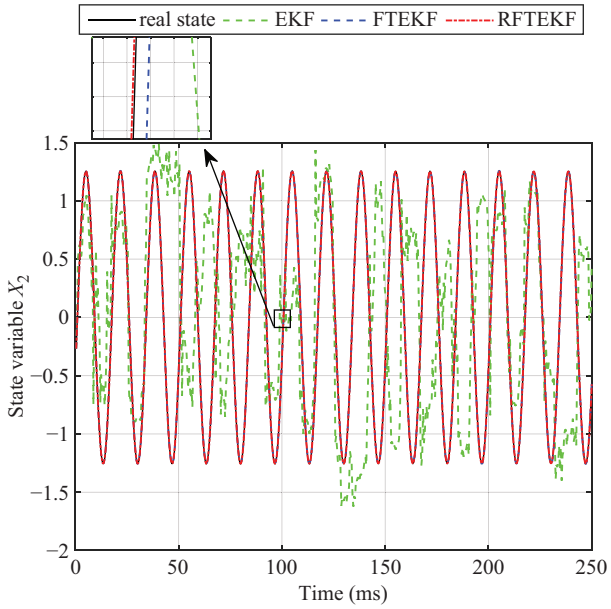

Fig. 12. Estimation results of state variable $\boldsymbol{x}_2$ by different methods.

TABLE II
PERFORMANCE COMPARISON

Metric	EKF	FTEKF	RFTEKF
E_{X_1}	0.4781	0.0820	0.0025
E_{X_2}	1.2071	0.0890	0.0050
E_{X_3}	0.5236	0.0066	0.0021
E_{X_4}	1.1847	0.0580	0.0041
E_{X_5}	0.2166	0.049	0.0018

Furthermore, synchronous estimation experiments were carried out to track the phase angle and amplitude of dynamic positive sequence voltage in the WECC test system using the traditional EKF, FTEKF, and the developed RFTEKF method. The comparison outcomes of the methods are shown in Figs. 16 and 17.

As demonstrated by the experimental results displayed in

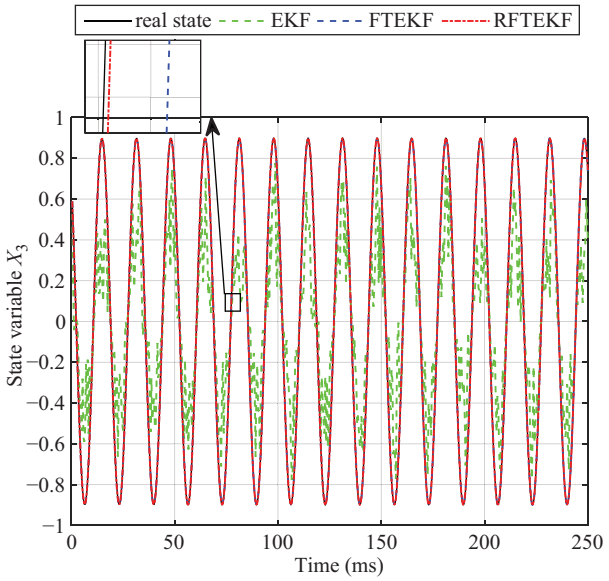

Fig. 13. Estimation results of state variables $\boldsymbol{x}_3$ by different methods.

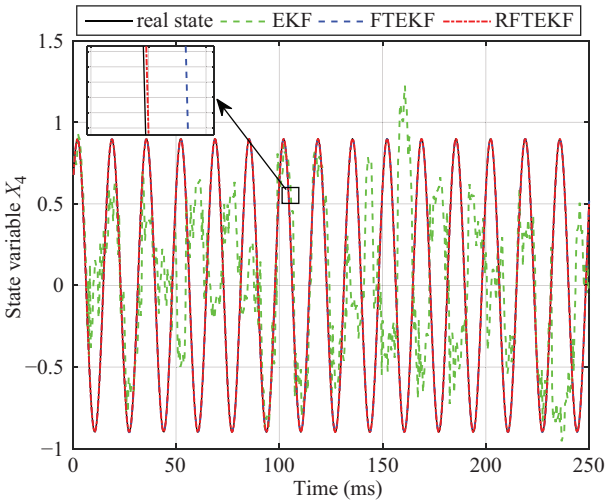

Fig. 14. Estimation results of state variables $\boldsymbol{x}_4$ by different methods.

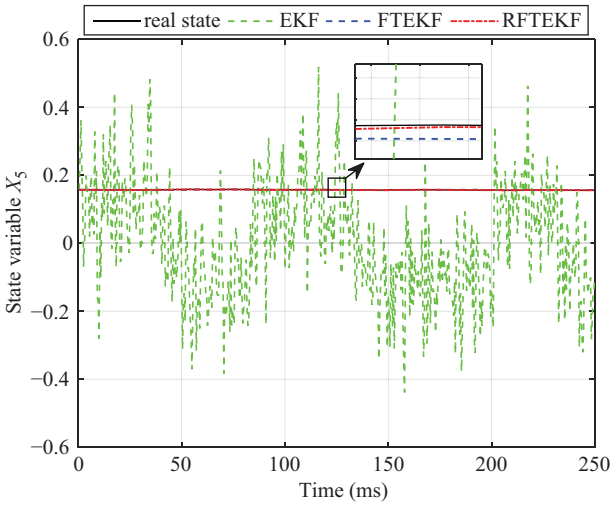

Fig. 15. Estimation results of state variable $\boldsymbol{x}_5$ by different methods.

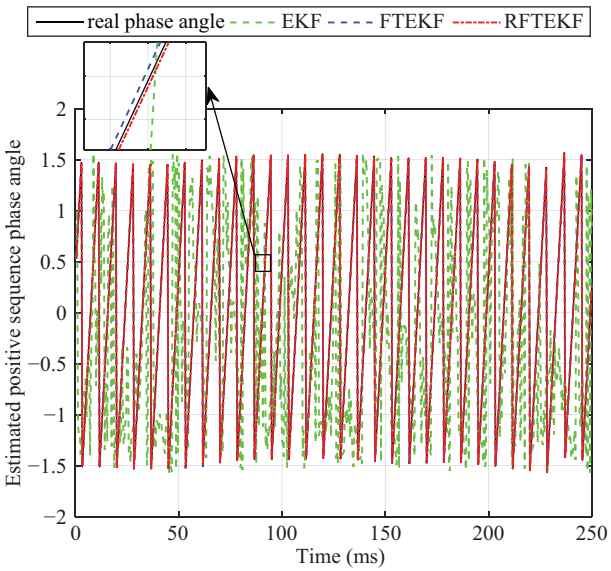

Fig. 16. Estimation result of positive sequence phase angle by different methods.

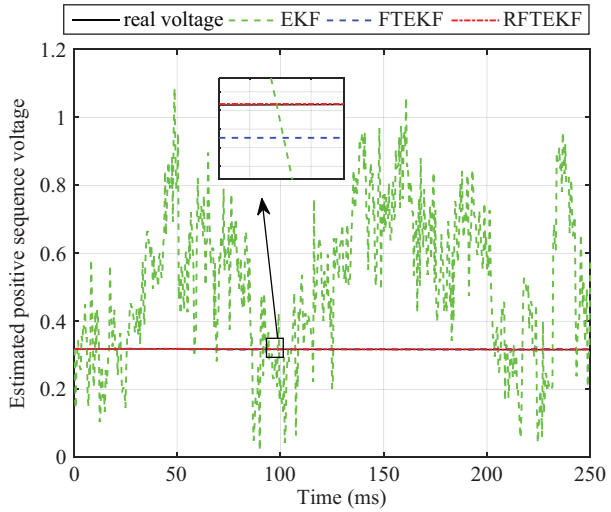

Fig. 17. Estimation result of positive sequence voltage magnitude by different methods.

Figs. 16 and 17, the estimation results of the traditional Kalman filter deviate largely from the true value of the voltage in the presence of partial missing measurements. The tracking effect of FTEKF is better than EKF because it considers the problem of missing measurements but only uses statistical characteristics, so the tracking effect is slightly inferior to RFTEKF. By contrast, the proposed RFTEKF can accurately track the amplitude and phase angle of the positive sequence voltage even with incomplete measurement information, displaying significantly improved performance over the conventional EKF method and FTEKF. In addition, the performance indicators of the three methods are provided in Table III, and the obvious deviation of the proposed RFTEKF approach is much smaller. These numerical results are consistent with those reflected in Figs. 16 and 17, which further confirms the proposed RFTEKF method is more robust and resilient in the case of partial missing measurements.

TABLE III
PERFORMANCE COMPARISON

Metric	EKF	FTEKF	RFTEKF
$E_{\hat{\theta}_p}$	1.2819	0.0098	0.0010
$E_{\hat{V}_p}$	0.2949	0.0080	0.0002

D. Case Study 3: Real Power System With DPGS Test

In this scenario, a signal from the actual power system with DPGS penetration in Henan Province, China, is considered. Specifically, the three-phase voltage at the 35KV bus bar near the wind-driven generator connection point is utilized and tested. The sampling frequency is 10,000 Hz and the simulation time is 1 s. In the application process, the initial covariance of state error is set as $10^{-6}\boldsymbol{I}_{n\times n}$, and the covariance of process and measurement noise is $\boldsymbol{Q}_0 = 10^{-10}\boldsymbol{I}_{5\times 5}, \boldsymbol{R}_0 = 10^{-10}\boldsymbol{I}_{5\times 5}$ respectively.

Figures 18 and 19 show measurement variables y_1 and y_2 with and without partial measurement missing information, respectively. Under the condition of partial measurement missing, we use three algorithms to estimate the power grid voltage data synchronously.

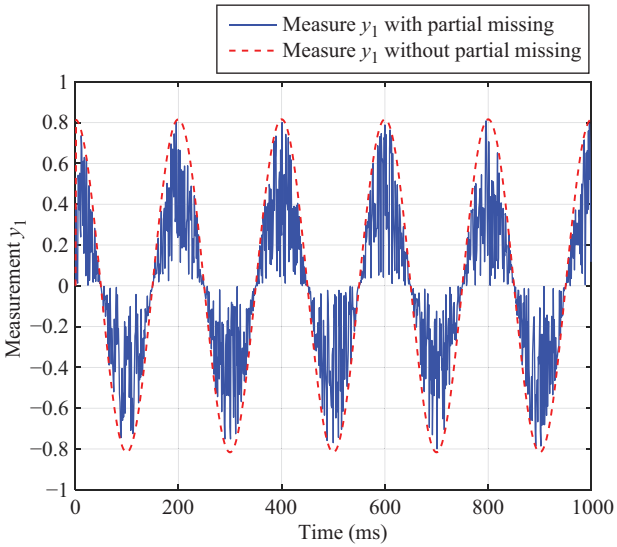

Fig. 18. Measurement y_1 with and without partial missing.

In Figs. 20–21, the results of grid synchronization estimation using voltage data collected at the point of interconnection of a wind turbine are shown. Only the tracking effect of voltage amplitude and phase angle are shown.

The experimental results show that the conventional EKF method seriously deviates from the true value trajectory since it was not designed with the effect of partial missing measurements. By contrast, the RFTEKF and FTEKF methods can obtain higher accuracy for state estimation. In addition, due to the proposed RFTEKF approach using the time-stamp technology to get packet loss information, the estimation error of RFTEKF is minimal. These estimation results further confirm the strong robustness of the RFTEKF against partial missing measurements and demonstrate its good scalability.

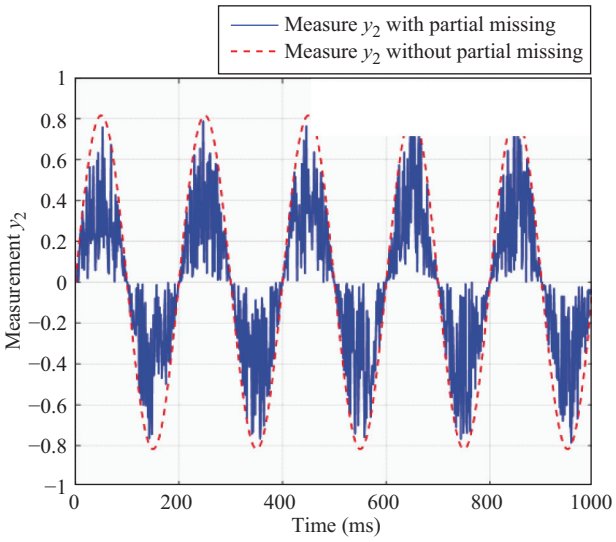

Fig. 19. Measurement y_2 with and without partial missing.

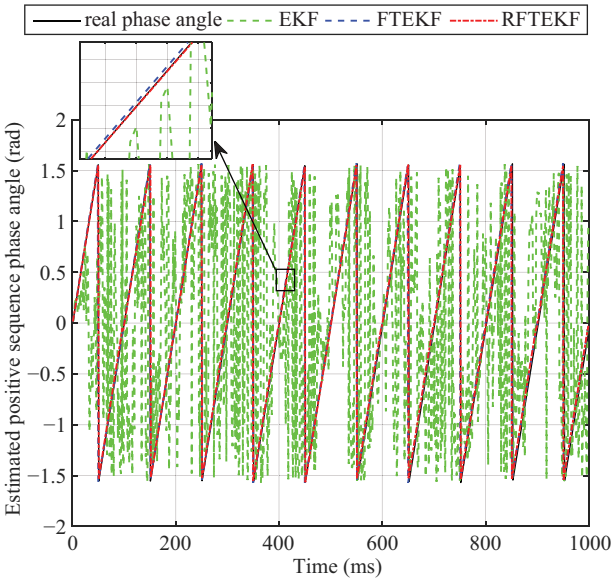

Fig. 20. Estimation result of positive sequence phase angle by different methods.

E. Case Study 4: Evaluation of Computational Efficiency

To satisfy various real-time energy management systems (EMS) applications, the estimation approach for smart grid synchronization needs to be computationally efficient. As a result, to determine whether the computation time of RFTEKF presented in this paper is lower than the PMU sampling rate, the entire running time of the conventional EKF, FTEKF and RFTEKF for the Case Study 1, Case Study 2 and Case Study 3 are calculated, and the results are displayed in Fig. 22. It can be seen from the calculation time the RFTEKF method has similar computational efficiency to FTEKF. Because of the complicated formula in the update stage, the operating time of RFTEKF is slightly longer than that of FTEKF. However, it is still lower than the sampling rate of the PMU. Therefore, the proposed RFTEKF method can satisfy the requirements for real-time tracking of smart grid synchronization estimation.

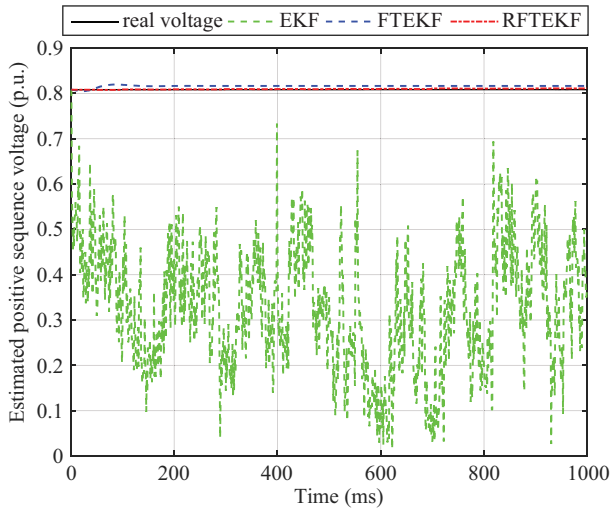

Fig. 21. Estimation result of positive sequence voltage magnitude by different methods.

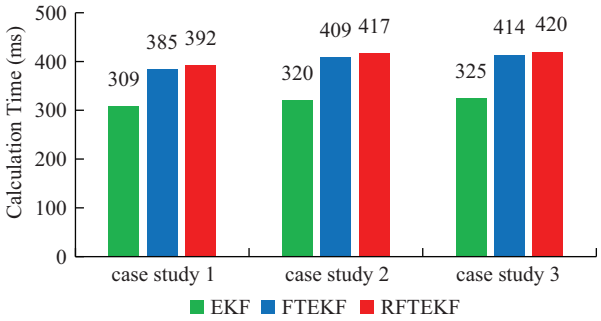

Fig. 22. Total execution time of each discussed approach for different test systems.

V. Conclusion

Accurate voltage synchronization under bad data, fault and distorted voltage conditions is critical for properly controlling electrical energy transfer between a distributed power generation system (DPGS) and the grid. In this article, lost information is considered to be known online using the time-stamp technique, and the gain is calculated by using its statistical characteristic to design and implement the estimator, which can effectively reduce the influence of partial loss of sensor data on state accuracy. Experimental data manifest that the proposed RFTEKF algorithm is robust and reliable for synchronous dynamic estimation of smart grid for various test systems with partial missing measurements. In future studies, we will focus on the collection of measurement data, as well as the analysis of statistical characteristics of the data.

References

[1] O. P. Mahela, M. Khosravy, N. Gupta, B. Khan, H. H. Alhelou, R. Mahla, N. Patel, and P. Siano, "Comprehensive overview of multi-agent systems for controlling smart grids," *CSEE Journal of Power and Energy Systems*, vol. 8, no. 1, pp. 115–131, Jan. 2022.

[2] J. Sun, M. J. Li, Z. G. Zhang, T. Xu, J. B. He, H. J. Wang, and G. H. Li, "Renewable energy transmission by HVDC across the continent: system challenges and opportunities," *CSEE Journal of Power and Energy Systems*, vol. 3, no. 4, pp. 353–364, Dec. 2017.

[3] G. Rietveld, J. P. Braun, R. Martin, P. Wright, W. Heins, N. Ell, P. Clarkson, and N. Zisky, "Measurement infrastructure to support the reliable operation of smart electrical grids," *IEEE Transactions on Instrumentation and Measurement*, vol. 64, no. 6, pp. 1355–1363, Jun. 2015.

[4] A. A. Kebede, T. Kalogiannis, J. Van Mierlo, and M. Berecibar, "A comprehensive review of stationary energy storage devices for large scale renewable energy sources grid integration," *Renewable and Sustainable Energy Reviews,* vol. 159, pp. 112213, May 2022, doi: 10.1016/j.rser.2022.112213.

[5] V. Kekatos and G. B. Giannakis, "Distributed robust power system state estimation," *IEEE Transactions on Power Systems*, vol. 28, no. 2, pp. 1617–1626, May 2013.

[6] A. Sahoo, K. Mahmud, and J. Ravishankar, "An enhanced frequency-adaptive single-phase grid synchronization technique," *IEEE Transactions on Instrumentation and Measurement*, vol. 70, pp. 9002611, Apr. 2021.

[7] Z. X. Zou, X. Q. Liu, J. Tang, G. De Carne, M. Liserre, Z. Wang, and M. Cheng, "Power synchronization of smart transformers allowing universal operation in radial and meshed grids," *CSEE Journal of Power and Energy Systems*, doi: 10.17775/CSEEJPES.2021.02350

[8] B. C. Babu, K. Sridharan, E. Rosolowski, and Z. Leonowicz, "Analysis of SDFT based phase detection system for grid synchronization of distributed generation systems," *Engineering Science and Technology, an International Journal*, vol. 17, no. 4, pp. 270–278, Dec. 2014.

[9] H. Saxena, A. Singh, J. N. Rai, and M. Badoni, "PV integrated grid synchronization technique using modified SOGI-FLL and zero-crossing detector," *Electrical Engineering*, vol. 104, no. 3, pp. 1361–1372, Jun. 2022, doi: 10.1007/s00202-021-01394-3.

[10] H. D. Sun, S. Y. Wang, S. Y. Xu, J. T. Bi, and Y. M. Wang, "Synchronization stability analysis of PLL-based grid-connected VSC system by voltage space vectors," *CSEE Journal of Power and Energy Systems*, to be published. DOI: 10.17775/CSEEJPES.2022.04450

[11] A. Bamigbade and V. Khadkikar, "Parameter estimation and grid synchronization using a first-order frequency-locked loop," *IEEE Transactions on Instrumentation and Measurement*, vol. 71, pp. 6500113, Jan. 2022.

[12] K. Sridharan and B. C. Babu, "A novel adaptive bandpass filter based PLL for grid synchronization under distorted grid conditions," *IEEE Transactions on Instrumentation and Measurement*, vol. 71, pp. 9003111, Apr. 2022.

[13] A. Sahoo, J. Ravishankar, and C. Jones, "Phase-Locked loop independent second-order generalized integrator for single-phase grid synchronization," *IEEE Transactions on Instrumentation and Measurement*, vol. 70, pp. 9004409, Aug. 2021.

[14] J. He and S. X. Duan, "Open-loop phase synchronization method of positive and negative sequences for three-phase asymmetric grid," *CSEE Journal of Power and Energy Systems*, vol. 9, no. 5, pp. 1973–1979, Sep. 2023, doi: 10.17775/CSEEJPES.2021.08600.

[15] L. Zhao and A. Abur, "Multi area state estimation using synchronized phasor measurements," *IEEE Transactions on Power Systems*, vol. 20, no. 2, pp. 611–617, May 2005.

[16] A. S. Debs and R. E. Larson, "A dynamic estimator for tracking the state of a power system," *IEEE Transactions on Power Apparatus and Systems*, vol. PAS-89, no. 7, pp. 1670–1678, Sep. 1970.

[17] J. B. Zhao and L. Mili, "A framework for robust hybrid state estimation with unknown measurement noise statistics," *IEEE Transactions on Industrial Informatics*, vol. 14, no. 5, pp. 1866–1875, May 2018.

[18] Y. Q. Wang, Z. W. Yang, Y. Wang, V. Dinavahi, J. Liang, and K. W. Wang, "Robust dynamic state estimation for power system based on adaptive cubature Kalman filter with generalized correntropy loss," *IEEE Transactions on Instrumentation and Measurement*, vol. 71, pp. 9003811, May 2022.

[19] G. Cheng, Y. Z. Lin, Y. B. Chen, and T. S. Bi, "Adaptive state estimation for power systems measured by PMUs with unknown and time-varying error statistics," *IEEE Transactions on Power Systems*, vol. 36, no. 5, pp. 4482–4491, Sep. 2021.

[20] C. Ren, Y. Xu, J. H. Zhao, R. Zhang, and T. Wan, "A super-resolution perception-based incremental learning approach for power system voltage stability assessment with incomplete PMU measurements," *CSEE Journal of Power and Energy Systems*, vol. 8, no. 1, pp. 76–85, Jan. 2022.

[21] L. Peng, Y. B. Li, L. Mili, Y. Tang, Y. J. Xu, B. Zhao, and J. J. Li, "A real-time enhanced thevenin equivalent parameter estimation method for PLL synchronization stability control in VSC," *IEEE Transactions on Power Delivery*, vol. 37, no. 4, pp. 2650–2660, Aug. 2022.

[22] D. R. Ding, Z. D. Wang, B. Shen, and H. L. Dong, "Envelope-constrained H_∞ filtering with fading measurements and randomly occurring nonlinearities: the finite horizon case," *Automatica*, vol. 55, pp. 37–45, May 2015.

[23] J. Q. Lin, H. C. Wu, and S. C. Chan, "A new regularized recursive dynamic factor analysis with variable forgetting factor and subspace dimension for wireless sensor networks with missing data," *IEEE Transactions on Instrumentation and Measurement*, vol. 70, pp. 9509713, May 2021.

[24] L. Hu, Z. D. Wang, I. Rahman, and X. H. Liu, "A constrained optimization approach to dynamic state estimation for power systems including PMU and missing measurements," *IEEE Transactions on Control Systems Technology*, vol. 24, no. 2, pp. 703–710, Mar. 2016.

[25] B. G. Qu, B. Shen, Y. X. Shen, and Q. Li, "Dynamic state estimation for islanded microgrids with multiple fading measurements," *Neurocomputing*, vol. 406, pp. 196–203, Sep. 2020.

[26] X. L. Jiang and G. H. Xia, "Nonfragile formation control of leaderless unmanned surface vehicles with memory sampling data and packet loss," *IEEE Systems Journal*, vol. 17, no. 2, pp. 3026–3035, Jun. 2023.

[27] D. Kumar, "Islanding detection in microgrid compromising missing values using NI sensors," *IEEE Systems Journal*. vol. 16, no. 2, pp. 1786–1795, Jun. 2022.

[28] B. Hu, H. J. Wang, T. Niu, C. Z. Shao and C. Y. Li, "Multi-time-scale coordinated optimal dispatch of virtual power plant under unreliable communication," *CSEE Journal of Power and Energy Systems*, doi: 10.17775/CSEEJPES.2021.00650.

[29] Y. Wang, L. W. Xu, F. J. Zhang, H. X. Dong, Y. Liu, and G. D. Yin, "An adaptive fault-tolerant EKF for vehicle state estimation with partial missing measurements," *IEEE/ASME Transactions on Mechatronics*, vol. 26, no. 3, pp. 1318–1327, Jun. 2021.

[30] J. Hu, Z. D. Wang, F. E. Alsaadi, and T. Hayat, "Event-based filtering for time-varying nonlinear systems subject to multiple missing measurements with uncertain missing probabilities," *Information Fusion*, vol. 38, pp. 74–83, Nov. 2017.

[31] X. Wang and E. E. Yaz, "Second-Order fault tolerant extended Kalman filter for discrete time nonlinear systems," *IEEE Transactions on Automatic Control*, vol. 64, no. 12, pp. 5086–5093, Dec. 2019.

[32] X. Wang and E. E. Yaz, "Smart power grid synchronization with fault tolerant nonlinear estimation," *IEEE Transactions on Power Systems*, vol. 31, no. 6, pp. 4806–4816, Nov. 2016.

[33] T. Mori, N. Fukuma, and M. Kuwahara, "Explicit solution and eigenvalue bounds in the Lyapunov matrix equation," *IEEE Transactions on Automatic Control*, vol. 31, no. 7, pp. 656–658, Jul. 1986.

[34] D. Simon, Optimal State Estimation: Kalman, H_∞, and Nonlinear Approaches, Hoboken, NJ, USA: Wiley, 2006.

[35] Y. Wang, Y. Q. Wang, Y. H. Sun, V. Dinavahi, J. Liang, and K. W. Wang, "Resilient dynamic state estimation for multi-machine power system with partial missing measurements," *IEEE Transactions on Power Systems*, vol. 39, no. 2, pp. 3299–3309, Mar. 2024, doi: 10.1109/TPWRS.2023.3287151.

[36] F. Naseri, E. Schaltz, D. I. Stroe, A. Gismero, and E. Farjah, "An enhanced equivalent circuit model with real-time parameter identification for battery state-of-charge estimation," *IEEE Transactions on Industrial Electronics*, vol. 69, no. 4, pp. 3743–3751, Apr. 2022.

[37] T. Gao, J. D. Duan, J. Z. Qiu, and W. T. Ma, "Robust forecasting-aided state estimation of power system based on extended Kalman filter with adaptive kernel risk-sensitive loss," *International Journal of Electrical Power & Energy Systems*, vol. 147, pp. 108809, May 2023, doi: 10.1016/J.IJEPES.2022.108809.

[38] G. Özkurt and E. Zerdali, "Design and implementation of hybrid adaptive extended Kalman filter for state estimation of induction motor," *IEEE Transactions on Instrumentation and Measurement*, vol. 71, pp. 7500212, Jan. 2022.

[39] B. Sinopoli, L. Schenato, M. Franceschetti, K. Poolla, M. I. Jordan, and S. S. Sastry, "Kalman filtering with intermittent observations," *IEEE Transactions on Automatic Control*, vol. 49, no. 9, pp. 1453–1464, Sep. 2004.

[40] H. S. Zhang, X. M. Song, and L. Shi, "Convergence and mean square stability of suboptimal estimator for systems with measurement packet dropping," *IEEE Transactions on Automatic Control*, vol. 57, no. 5, pp. 1248–1253, May 2012.

Yi Wang received his B.S. degree from Luoyang Institute of Science and Technology, Luoyang, China, in 2014; and received his Ph.D. degree from Hohai University, Nanjing, China, in 2020. He was a visiting scholar at the University of Alberta between 2018 and 2019. He is an Associate Professor at Zhengzhou University, and a Henan Province Outstanding Youth Fund winner. His research interests include theoretical and algorithmic studies in power system estimation, parameter identification, power system dynamics, signal processing, and cyber security. He is also an active reviewer for many international journals.

Yanxin Liu received her B.S. degree in Electric Power System and Its Automation from Zhongyuan University of Technology, Zhengzhou, China, in 2022. She is pursuing an M.S. degree in Electrical Engineering at Zhengzhou University, Zhengzhou, China. Her research interests include theoretical and algorithmic studies in power system estimation.

Mingdong Wang received his Ph.D. degree from Harbin Institute of Technology, Harbin, China, in 2008. He is a Professor at Zhengzhou University. His research interests are power system analysis and control, intelligent theory and application in power systems. He is also an active reviewer for many international journals.

Venkata Dinavahi received the B.Eng. degree in Electrical Engineering from Visvesvaraya National Institute of Technology (VNIT), Nagpur, India, in 1993, the M.Tech. degree in Electrical Engineering from the Indian Institute of Technology (IIT) in Kanpur, India, in 1996 and the Ph.D. degree in Electrical and Computer Engineering from the University of Toronto, Ontario, Canada, in 2000. He is a Professor at the Department of Electrical and Computer Engineering, University of Alberta, Edmonton, Alberta, Canada. He is a Fellow of the Engineering Institute of Canada. His research interests include real-time simulation of power systems and power electronic systems, electromagnetic transients, device-level modeling, large-scale systems, and parallel and distributed computing.

Jun Liang received his B.S. degree in Electric Power Systems and Its Automation from the Huazhong University of Science and Technology, Wuhan, China, in 1992, and his M.S. and Ph.D. degrees in Electric Power System and Its Automation from China Electric Power Research Institute (CEPRI), Beijing, in 1995 and 1998, respectively. From 1998 to 2001, he was a Senior Engineer with CEPRI. From 2001 to 2005, he was a Research Associate with Imperial College London, U.K. From 2005 to 2007, he was with the University of Glamorgan, Pantiplife, U.K., as a Senior Lecturer. He is currently a Professor of Power Electronics at the School of Engineering, Cardiff University, Cardiff, U.K. His research interests include HVDC, MVDC, FACTS, power system stability control, power electronics, and renewable power generation. Prof. Liang is a Fellow of the Institution of Engineering and Technology (IET). He is the Chair of IEEE UK and Ireland Power Electronics Chapter. He is an Editorial Board Member of CSEE JPES. He is an Editor of the IEEE Transactions on Sustainable Energy.

Yonghui Sun received the Ph.D. degree from the City University of Hong Kong, Hong Kong, China, in 2010. He is a Professor at the College of Energy and Electrical Engineering, Hohai University, Nanjing, China. He has authored more than 100 papers in refereed international journals. His research interests include stability analysis and control of power systems, optimal planning and operation of integrated energy system, optimization algorithms, and data analysis. Dr. Sun received the First Award of Jiangsu Provincial Progress in Science and Technology in 2010 as the Fourth Project Member. He is an active reviewer for many international journals.